Lipid binding attenuates channel closure of the outer membrane protein OmpF

Authors

Idlir Liko[1,2], Matteo T. Degiacomi[1†‡], Sejeong Lee[1‡], Thomas D. Newport[2], Joseph Gault[1], Eamonn Reading[1⊥], Jonathan T.S. Hopper[1,2], Nicholas G. Housden[3], Paul White[3], Matthew Colledge[4], Altin Sula[4], Bonnie A. Wallace[4], Colin Kleanthous[3], Phillip J. Stansfeld[3], Hagan Bayley[1], Justin L.P. Benesch[1], Timothy M. Allison[1*˙] and Carol V. Robinson[1,2*]

1 Department of Chemistry, University of Oxford, South Parks Road, Oxford, OX1 5QY, UK

2 OMass Technologies, Begbroke Science Park, Kidlington, OX5 1PF, UK

3 Department of Biochemistry, University of Oxford, South Parks Road, Oxford, OX1 3QU, UK

4 Institute of Structural and Molecular Biology, Birkbeck College, University of London, Malet Street, London, WC1E 7HX, UK

⊥ Current address: Department of Chemistry, Kings College London, Britannia House, 7 Trinity Street, London, WC2R 2LS, UK

† Current address: Chemistry Department, Durham University, South Road, Durham, DH1 3LE, UK

˙ Current address: Biomolecular Interaction Centre and School of Physical and Chemical Sciences, University of Canterbury, Christchurch, NZ

‡ These authors contributed equally to this work

Abstract

Strong interactions between lipids and proteins occur primarily through association of charged head-groups and amino-acid side-chains, rendering the protonation status of both partners important. Here we use native mass spectrometry (MS) to explore lipid binding as a function of charge of the outer membrane porin F (OmpF). We find that binding of anionic phosphatidylglycerol (POPG) or zwitterionic phosphatidylcholine (POPC) to OmpF is sensitive to electrospray polarity while the effects of charge are less pronounced for other proteins in outer or mitochondrial membranes: the ferripyoverdine receptor (FpvA) or the voltage-dependent anion channel (VDAC). Only marginal charge-induced differences were observed for inner membrane proteins: the ammonia channel (AmtB) or the mechanosensitive channel (MscL). To understand these different sensitivities we performed extensive bioinformatics analysis of membrane protein structures and found that OmpF, and to a lesser extent FpvA and VDAC, have atypically high local densities of basic and acidic residues in their lipid headgroup binding regions. Coarse-grained molecular dynamics simulations, in mixed lipid bilayers, further implicate changes in charge by demonstrating preferential binding of anionic POPG over zwitterionic POPC to protonated OmpF, an effect not observed to the same extent for AmtB. Moreover electrophysiology and mass spectrometry-based ligand binding experiments, at low pH, show that POPG can maintain OmpF channels in open conformations for extended time periods. Since the outer membrane is composed almost entirely of anionic lipopolysaccharide, with similar headgroup properties to POPG, such anionic lipid binding could prevent closure of OmpF channels thereby increasing access of antibiotics that use porin-mediated pathways.

Significance

Outer membrane porins are often considered as passive conduits of small molecules across lipid bilayers. Using native mass spectrometry experiments we identify a pH-sensitive lipid binding mechanism of OmpF, which enables increased threading of a colicin-derived peptide through open channels. Supported by molecular dynamics simulations and channel recording experiments, we posit that this mechanism attenuates channel opening in response to changes in environmental conditions, specifically pH. These findings have important consequences not only for mass spectrometry experiments, wherein the role of charge is often overlooked, but they also could be insightful for antibiotics that gain access to Gram-negative bacteria through porin mediated pathways.

Introduction

The outer membrane porin OmpF supports passive diffusion of small molecules through the outer membrane. Historically this trimeric protein was considered to exist only in an open form. As a consequence, permeation through outer membranes was thought to be regulated by modulating the cellular expression level of OmpF or the concertation of charged molecules. Surprisingly, despite its outer membrane location, little or no information is available on its interactions with lipids. Given that previous studies have implicated specific lipids in protein function {Heginbotham, 1998 #1056;Valiyaveetil, 2002 #1057;Starling, 1996 #1058;Dalton, 1998 #1059;Pilot, 2001 #1060;Powl, 2008 #1061} we were curious to know if such lipid binding sites exist on OmpF, and if so, where they are located and how they might change as a function of pH.

Studies of the distribution of lipid binding sites in membrane proteins have shown that the interactions of lipid head groups with a protein are important determinants for lipid binding {Powl, 2008 #1062;Hakizimana, 2008 #1063;Soubias, 2010 #1064;Vorobyov, 2011 #1101}. Accordingly charged amino acids are more likely to be positioned in areas of the protein surface that could interact with lipid head groups rather than in hydrophobic transmembrane regions {Ulmschneider, 2001 #1035;von Heijne, 2006 #1046}. It has also been suggested that along with physical bilayer properties, charges at protein-lipid interfaces, and the specific locations of amino acids, will play important roles in the interactions of membrane proteins with lipids {Contreras, 2011 #425}. Consistent with this, most X-ray crystal structures of membrane proteins, in which lipids have been resolved and modelled, show that the lipid-protein interactions are stabilized by polar interactions between lipid head groups and amino acids on the proteins {Morita, 2011 #1033;Contreras, 2011 #425;Norimatsu, 2017 #1097;Palsdottir, 2004 #1102}. Annular lipid binding may also occur through charge-based interactions between the protein and the lipid head group but in general this type of interaction is more difficult to define given the diffusive nature of the lipid environment.

Native mass spectrometry (MS) has proven useful for studying both specific membrane protein-lipid interactions {Landreh, 2016 #1051;Marcoux, 2013 #1020;Liko, 2016 #1098;Allison, 2015 #1026;Laganowsky, 2014 #920;Liko, 2016 #1100} and the annular belts that surround membrane proteins {Bechara, 2015 #1052;Bechara, 2015 #1099}. While the precise mechanistic details of the electropray process are still under investigaton the generel consensus that emerges is that protein-lipid complexes acquire charge which is proportional to their solvent accessible surface area {Benesch, 2006 #244}. Early in the ionisation process, in transition from solution to the gas phase, and before final charge deposition, lipids that could carry a charge in a given polarity (for instance PC in positive electrospray polarity) may serve as a charge carrier {Hogan, 2009 #2414}. Effectively this means that during the desolvation process, if the protein has sufficiently high charge, it will relieve Coulombic repulsion through expulsion of charged carriers. This, we postulate, is observed as the reduction in lipid binding in certain combinations of protein, lipid and electrospray polarity. Since charge underlies the electrospray process MS is particularly suited to investigating charge mediated interactions, such as those between the lipid head group and the corresponding region of the protein, electrostatic interactions being strengthened in the gas phase {Robinson, 1996 #988;Yin, 2008 #1048}. Charge-based interactions can be probed by MS through changes in the electrospray polarity under which ions are generated, analogous to changes in pH experienced in solution or *in vivo*. For instance, OmpF, along

with other outer membrane proteins, can tolerate pH changes in the range of pH 2 -7 {Foster, 2004 #1104}.

To validate and compare protein lipid binding properties of OmpF at different pHs we included additional proteins with different structural features and membrane locations: the ferripyoverdine receptor (FpvA) from *Pseudomonas aeruginosa,* also an outer membrane protein, and the voltage-dependent anion channel (VDAC) from *Homo sapiens* located in the mitochondrial membrane. Three inner membrane proteins were selected: the *E. coli* ammonia channel (AmtB) and the *Mycobacterium tuberculosis* mechanosensitive channel of large conductance (MscL) and the *Magnetococcus sp.* (strain MC-1) voltage-gated sodium channel (NavMs).

We compared the lipid binding properties of all six membrane proteins under different conditions, and developed a novel computational algorithm to define the lipid binding head group regions of all membrane proteins in the PDB. We then correlated changes in lipid binding properties with different charged residue distributions in the critical regions identified. We validated our findings with coarse-grained molecular dynamics simulations and single channel recording experiments. Together this integrative approach has allowed us to define a new role for specific lipid binding to OmpF at low pH: in maintaining open states of an outer membrane porin for increased passage of small molecules including antibiotics.

Results

Lipid binding to OmpF is sensitive to changes in the electrospray polarity

To investigate the sensitivity of lipid binding to OmpF, as a function of charge, we first purified the protein to remove remaining endogenous lipids. OmpF was then incubated with the anionic lipid POPG (10-fold excess over protein). Mass spectra in octyl glucoside (OG) were recorded in both positive and negative electrospray polarities (Fig. 1A and B). Additional adduct peaks on the charge state series for the OmpF trimer are assigned to binding of POPG. Surprisingly, when the electrospray polarity was switched to the negative ion mode, using the same protein-lipid solution and nano-electrospray tip, no POPG binding was observed. Selecting next the neutral zwitterionic lipid POPC, we found that for negatively charged OmpF, multiple POPC lipids (<4) could be observed bound to OmpF, while no binding was observed when the electrospray polarity was switched back to positive. These dramatic and clear cut changes in lipid binding as a function of charge were unprecedented.

To examine if this sensitivity to charge was a general phenomenon or specific to OmpF we selected AmtB, incubating it with POPC or POPG. In this case lipids could be observed bound both to positively or negatively charged protein with approximately equal intensity (Fig. 1C and D). Extending our investigations to MscL, a protein known to sense and respond to membrane tension {Iscla, 2012 #1106}, we found only a moderate difference in the extent of lipid binding in the spectra recorded under the two different polarities (Fig. S1). A further three membrane proteins were investigated: NavMS, FpvA and VDAC. For NavMS a low level of POPG was detected binding to negatively charged protein while POPC was observed bound only to negatively charged NavMS (Fig. S1). Intriguingly FpvA showed low levels of POPG binding, but high levels of binding to POPC (>3) when negatively charged (Figs. S1). MscL, on the other hand could be seen bound to POPC in both polarities, while

VDAC was only observed bound to POPC when negatively charged. Given that the same lipids were used in all experiments, and therefore subject to the same charging conditions, survival of the differing interactions must arise from the distribution of chargeable residues in the various proteins.

Plotting the extent of lipid binding as a function of the different electrospray polarities under which the six membrane proteins were investigated reveals three distinct categories (Fig. 1F): (1) those for which lipids were observed bound to approximately equal extent while positively or negatively charged (e.g. AmtB) (2) where lipids were observed bound in one electrospray polarity and noticeably less in the other (e.g. NavMS) and (3) where lipid binding was observed in one electrospray polarity but undetected in the other (e.g. OmpF).

In summary AmtB is an example of a protein that showed little change in lipid binding as a function of electrospray polarity whereas OmpF showed the greatest sensitivity. Comparing the electrostatic surfaces of the two proteins, generated at artificially low and high pH to mimic the positive and negative ion electrospray polarities of the mass spectrometer, a large shift in the charge carriers from acidic to basic residues was observed for OmpF whereas only a modest shift was observed for AmtB. We conclude that the dramatic changes in lipid binding arise as a function of the differing degrees of change, and distribution of charges, induced by protonation / deprotonation events (Fig. 1G).

Locating chargeable residues positioned for lipid binding

To see how charge density in the lipid head group binding region varied across a wide range of membrane proteins we exploited a database that predicts the alignment of all the transmembrane proteins currently available in the protein data bank (PDBTM) with a synthetic lipid bilayer {Berman, 2000 #1050}. We aligned 2063 structures according to PDBTM, and subsequently studied their surface in regions expected to interact with lipid head groups. We first simulated the predicted lipid head group regions of the membrane as two layers of mesh points. Any mesh point clashing with a protein atom or located in a protein internal cavity (e.g. a channel) was removed (Fig. 2A). We then calculated the solvent accessible surface area of all protein atoms within 4 Å from each mesh. The percentage of this surface featuring amino acids capable of picking up a positive charge (defined as "basic") or releasing one ("acidic") was then calculated.

We first determined the total surface percentage composed of basic or acidic residues for each protein using the two surface regions corresponding to the inside and outside of the protein (Fig. 2B). We found an average total for acidic residues of 27 ± 15 %, and for basic residues of 39 ± 17%. This wide range of values for both residue types suggests that there is a slight preference for basic residues. Next we determined whether different secondary structure leads to the presentation of specific lipid-interacting head groups. We therefore extracted from our dataset subsets of α-helical (1769 entries) and β-sheet (294) proteins. Interestingly, outer membrane proteins (which comprise almost exclusively the set of β-sheet proteins) typically have more acidic and basic residues than their inner membrane counterpats which are typically α-helical (Fig. 2B).

We then considered differences in residue composition on either side of the membrane. That is, whether a high relative surface area of either acidic or basic residues on one side of the protein was correlated with a large difference on the opposing side. Within the dataset

we found proteins where the distribution of chargeable residues was symmetric, and others where it was highly asymmetric (Figs. S2 and S3). This suggests that the residues interacting with the lipid head groups are not generally paired with potential bilayer asymmetries or affected by protein topology. Interestingly, some proteins (OmpF, VDAC and FpvA studied here) have a high contribution of chargeable residues in these surface areas. We hypothesise that these dense regions of highly charged residues lead to the observed lipid binding sensitivity associated with changes in protonation.

pH-sensitivity to lipid binding preferences

Working on the hypothesis that a high local density of acidic residues in OmpF will lose their negative charge to become neutral and thereby exhibit pH-sensitive lipid binding, we compared OmpF with AmtB *in silico* mimicking these low pH conditions. We set up a series of coarse-grained molecular dynamics simulations of both proteins in mixed bilayers comprised of equal quantities of POPC and POPG and mimicked both deprotonated and protonated states. To approximate protonation, negatively charged side-chain beads of aspartic and glutamic acid residues and negatively charged lipid phosphate groups were neutralised, and a positive charge was applied to a sidechain bead of each histidine.

Five separate 1-μs simulations were performed for both proteins in both states, and occupancy of POPG molecules as a fraction of total lipid occupancy (POPG and POPC) within 6 Å of the protein (corresponding to the first annular shell, Fig. S4) was measured for each acidic residue. Both AmtB and OmpF show an increase in POPG fraction in the protonated state, however POPG binding is substantially more pronounced in the case of OmpF (Figs. 3 and S5). In order to examine more localised changes in patterns of binding, we examined changes in the lipid binding preferences on a 2D grid over the upper and lower leaflets of each protein. In both cases, the net shift in lipid binding preferences comprises both local increases and decreases in POPG fraction, as would be expected (Fig. 3). In the case of OmpF, shifts occurring upon protonation differ greatly between leaflets, with OmpF in the upper leaflet attracting POPG and the lower leaflet shifting more towards POPC. However, for the latter, apparent changes in bulk lipid regions are less relevant, there remains a change in POPG in proximity to the acidic residues.

In summary, the simulations suggest that the positioning of acidic residues in the lipid headgroup-binding region of OmpF, particularly the upper leaflet, affect its lipid binding preference depending on protonation conditions. These molecular dynamics results corroborate the effects of acidic residues on lipid binding observed in our native MS experiments, suggesting that the high density of chargeable residues in OmpF affect lipid binding preferences in the context of a membrane bilayer.

POPG stabilises OmpF in an open conformation

Given the results from native MS and molecular dynamics simulations, that suggest that POPG-OmpF interactions persist at low pH, we examined the effect of POPG on the conductance and gating of OmpF. We reconstituted OmpF trimer in a planar lipid bilayer membrane, in which each monomer can be observed and lipid composition can be modulated {Bayley, 2001 #1103;Pliotas, 2015 #1107}. We first used symmetric bilayers of DPhPC, a lipid commonly used in planar lipid bilayer measurements with the same overall

neutral, zwitterionic head group as POPC, compared to the net negative charge of POPG. The mean unitary conductance of OmpF in a pure DPhPC bilayer was 1.3 ± 0.2 nS (n = 19) per monomer (Fig. 4A), identical to the known value {Nestorovich, 2003 #1104}. In the presence of 25% POPG at pH 4 the unitary conductance value increased slightly by 7% to 1.4 ± 0.1 nS (n = 15) (Fig. 4A), meanwhile at pH 8 the conductance value of OmpF remained unchanged in the presence of POPG (Fig. S6). This provided an initial suggestion that the presence of POPG in DPhPC bilayers may increase ion flow through OmpF in acidic conditions. .

To investigate the pore dynamics in more detail, channel gating was examined under the action of an applied potential at 100 mV. Due to the acidic conditions at pH 4, a voltage was applied that was lower than the critical voltage for closure (~ ±130 mV) {Baslé, 2004 #1105}. The characteristic three-step opening and closing of OmpF was monitored until all three subunits had closed - as indicated by a decrease in the current to almost zero (Figs. 4B and D). In DPhPC bilayers the mean closure time for OmpF from the fully open state (O3) to the fully closed state (C) was measured as 54.3 s (n = 11) by fitting to an exponential distribution. In the presence of POPG (25%) the mean closure time increased to 175.8 s (n = 10). This three-fold increase (*p*-value of 0.023) suggests that POPG helps to stabilise OmpF in an open state (Fig. 4C).

By examining the closure steps in more detail, the presence of POPG was specifically found to influence two closing steps (O2→O1 and O1→C) (Fig. S7 and Table S2). The mean closing time for these two steps also increased to be three-fold larger in the presence of POPG from 4.9 s to 13.1 s and from 17.9 s to 48 s, respectively (*p*-values 0.015 and 0.044, respectively) and a higher probability of re-opening (O2→O3 and O1→O2) was also observed (Fig. S8). In the presence of POPG the re-opening of single subunit closed state of OmpF (O2→O3) occurred for 70% of pores analysed (7/10), compared with only 10% (1/11 pores analysed) in the absence of POPG. Taken together, this indicates that the presence of POPG lipid in the membrane not only helps maintain an open pore conformation but promotes the reopening of closed pores. These quantitative analyses reveal that POPG influences the voltage-induced gating of OmpF at low pH, and promotes a three-fold change in the delay of closing.

Probing the open pores

Aside from its role in the passive diffusion of small molecules through the outer membrane, OmpF also forms part of a cytotoxic translocon complex, through which the nuclease colicin ColE9 threads to initiate cell entry and ultimately death {Housden, 2013 #983}. The intrinsically unstructured translocation domain of ColE9 has two OmpF binding sites in its sequence (OBS1 and OBS2), and these sequences as peptides can be observed to bind to OmpF inside the pores within the trimer. Access to the peptide binding sites inside the pores may be affected by the extracellular loops, and since the electrophysiology experiments clearly demonstrate a change in gating behaviour in the presence of POPG, we hypothesised that the OmpF-OBS1 interaction may also be influenced by POPG binding. Using high-resolution native MS {Gault, 2016 #1096} we analysed the relative binding of the OBS1 peptide to different lipid-bound forms of OmpF. Notably we observe that POPG-bound OmpF binds OBS1 more than POPG-free OmpF (Figs. 4E and S9), suggesting POPG increases the apparent affinity of the protein for the peptide. This direct evidence supports a

scenario where interactions between OmpF and POPG stabilise the open conformation of the pore. This suggests that *in vivo* OmpF function can be fine-tuned by lipid interactions.

Discussion

Building upon previous investigations {Powl, 2008 #1062;Hakizimana, 2008 #1063} we have shown that the head group interactions of lipids can play a role in the direct interaction of lipids with membrane proteins. As a corollary, the membrane protein surfaces that interact with lipid head groups can regulate the selectivity of lipid binding. Interestingly we found that different classes of membrane proteins have different distributions of acidic and basic residues in these binding areas. Outer membrane proteins tend to possess lipid head group binding surfaces comprised of a higher concentration of both acidic and basic residues, suggesting there may be more pronounced differences in lipid binding behaviour. Notably, in line with this, we found that membrane proteins with representatively high concentrations of acidic residues in these regions showed lipid binding by native MS that was dependent on the combination of lipid and electrospray polarity. Therefore, to probe membrane protein-lipid interactions by native MS, and to examine a full range of lipid binding interactions, an appropriate choice of electrospray polarity is necessary, and will be particularly important for proteins with high percentages of chargeable residues in the head group binding regions.

We probed how lipid binding preferences may differ in response to changing pH by molecular dynamics simulations, and electrophysiology experiments. OmpF has the greatest surface area of chargeable residues and showed the most differences in lipid binding as assessed by native MS, as well as enhanced POPG binding in molecular dynamics simulations. POPG binding to OmpF at single-channel level showed enhanced ion transport activity as indicated by the increase in conductance and the prolonged open state under applied potentials. This could result from the electrostatic interactions between the net negative charge of the lipid head group and the chargeable residues at the surface of OmpF {Samartzidou, 1998 #1084;Conlan, 2000 #1085;Pezeshki, 2009 #1086}. pH changes and mutations of charged residues in extracellular loops have been shown to affect the voltage-induced gating {Arbing, 2000 #1087;Arbing, 2001 #1088;Scheuring, 2002 #1089;Delcour, 2003 #1090;Nestorovich, 2003 #1104;Todt, 1992 #1092;Muller, 1999 #1093}. This supports the idea that the stabilised OmpF open state, in POPG-containing bilayers, is induced by electrostatic interactions leading to a conformational change of the extracellular surface of OmpF.

We observed that under low pH conditions, OmpF, which has a large proportion of acidic residues in its lipid head group binding region, can subtly change lipid binding preferences. This means that this protein could respond to pH changes by recruiting a different cohort of annular lipids, which in turn could affect their stability or function. Considering the composition of the lipids in the outer leaflet of the outer membrane of *E. coli* a high proportion of LPS is antcipated, with recent evidence also suggesting the presence of other anionic lipids {Rowlett, 2017 #1109;Glenwright, 2017 #1110}. Given that the headgroup chemistry of LPS is analogous to POPG under neutral, positive and nagative ion modes, (Figure S3) the charge effects of POPG binding are likely to be analogous to those of LPS binding. Using the effects of POPG as a mimetic for LPS we considered binding at low pH and further explored the effects of lipid binding on channel closing by binding of the

translocon-derived peptide OBS1. Results showed that the extent of peptide thrading through the open channels can be affected by the binding of the lipid POPG under low pH conditions. The stability and interactions of OmpF thus appear to be influenced by lipid binding. Since both POPG and LPS are without formal charge at low pH we propose that both lipids would enable channeos to remain open for extnded time periods enabling increased peptide threading.

Taken together these MS, computational, and conductivity measurements have therefore uncovered how lipids can regulate OmpF, through the ability of the techniques to highlight and explore the allosteric effects of lipid binding. The ability of OmpF closure to be modulated by lipid binding is likely an important feature of outer membrane permeability {Delcour, 2009 #1103}. The finding that lipids can regulate closure of OmpF is important therefore, since it may well increase penetration of antibiotics using porin-mediated pathways.

Methods

Protein expression and purification

Membrane proteins were expressed and purified as previously described {Laganowsky, 2013 #336;Laganowsky, 2014 #920;Reading, 2015 #1022;Bagnéris, 2013 #1072;Housden, 2013 #983;White, 2017 #1109;Hiller, 2008 #1108}. These proteins were further purified to remove lipids present from the expression host. Prior to MS measurements proteins were buffer-exchanged into 200 mM ammonium acetate in the presence of twice the critical micelle concentration of C8E4 for AmtB, MscL and VDAC, OG for FpvA and OmpF, and HEGA-10 for the NavMs-pore.

Analysis of lipid head group binding regions of membrane protein structures

We exploited PDBTM {Kozma, 2013 #1049} to obtain information about membrane proteins amino acids exposed to lipid head groups. This database lists 2387 transmembrane proteins (June 2015) featured in PDB databank, providing information about their alignment in membrane, and the operations required to reconstitute their biological entity from the crystal structure. These include chain selections, transformation matrices and biomatrix operations needed to obtain a biological assembly aligned along the z axis (bilayer on the xy plane, z=0 being its center). The database also provides information about half bilayer thickness, hereon z_{PDBTM}. Entries in the database are categorized as being either α-helical or β-sheet proteins. The proteins categorized as β-sheet that were not already categorized as outer membrane based on PDB keywords were manually assigned.

In our analysis we considered only proteins having more than one strand crossing the bilayer, and excluded non-experimental models, which reduced the database to 2063 entries. After aligning the biological assemblies according to PDBTM, we quantified their amount of "basic" (Lys, Tyr, Cys, His) and "acidic" (Glu, Asp) residues that would be in contact with lipid head groups. Full details of the method applied independently to the outer and leaflet are described in Supplementary Methods.

Calculation of electrostatic potentials

Water and other ligands were first removed from all proteins' PDB files. PDB files used were: AmtB 4NH2 {Laganowsky, 2014 #920}, FpvA 2O5P {Brillet, 2007 #1080}, MscL 2OAR {Chang, 1998 #816}, NavMS 3ZJZ {Bagnéris, 2013 #1072}, OmpF 3POX {Efremov, 2012 #1082}, VDAC 2JK4 {Bayrhuber, 2008 #1083}. For every protein structure, protonation states at pH 1 and 12 were obtained using PDB2PQR {Dolinsky, 2004 #1094}. Van der Waals radii and partial charges were assigned to every atom according to the AMBER force field. Electrostatic potentials for all resulting protonated structures were then calculated using APBS {Baker, 2001 #1095}, with 1.4 Å solvent radius and a temperature of 300K. The dielectric constant was set to 80. While this will not accurately reproduce the electrostatic potential in the transmembrane region, it is suitable for the examination of solvent exposed regions neighboring lipid heads. Electrostatic potential surfaces were visualized casting the electrostatic volumetric information onto solvent accessible surfaces calculated with VMD.

Native MS

Lipids were purchased from Avanti Polar Lipids (Alabaster, AL, USA) and aliquots were prepared as described elsewhere {Laganowsky, 2014 #920} and stored as stock solution at 1 mg ml^{-1} at -20 °C.

Membrane proteins were introduced into a Synapt G1 (Waters, UK) (modified for high mass) using gold-coated capillaries prepared in-house {Hernandez, 2007 #146}. Cone and capillary voltages were respectively typically 1.4 kV and 180 V in positive ion mode, and -1.1 V and -160 V in negative ion mode. For improved transmission of large ions a backing pressure of 4.5–5.5 mbar was applied in the source region {Landreh, 2015 #1076;Tahallah, 2001 #268;Sobott, 2002 #270;Schmidt, 2001 #1077}. Collision voltage on the trap was varied between 130 V and 180 V and the same collision voltage was maintained in experiments comparing binding ratios between polarities. The activation voltage in the transfer region was maintained at 50 V thought out all measurements. MS data analysis was performed using MassLynx.

High Resolution Native MS

High resolution native MS was performed as described elsewhere {Gault, 2016 #1096}. Briefly, ions were introduced into a Q Exactive hybrid quadrupole-Orbitrap mass spectrometer (Thermo Fisher Scientific, Bremen Germany) modified for the transmission and detection of high mass ions {Rose, 2012 #272} and optimised for native MS of membrane protein complexes {Gault, 2016 #1096}. All spectra were acquired in "Native Mode" with maximum RF applied to all ion optics, -3.2 kV to the central electrode of the Orbitrap and with ion trapping in the HCD cell. Ions were generated in the positive ion mode from a static nanospray source using gold-coated capillaries prepared in-house {Hernandez, 2007 #146}. Ions then passed through a temperature controlled transfer tube (40–80 °C), RF-lens, injection flatapole and bent flatapole. After traversing the selection quadrupole, which was operated with a wide selection window (1,000–20,000 m/z), ions were trapped in the HCD cell before being transferred into the C-trap and Orbitrap mass analyser for detection. Transient times were 64 ms and AGC target was 1×10^6. Spectra were acquired with 10 microscans, averaged over 50–100 scans and with a noise level parameter set to 3, slightly lower than the default of 4.68 in order to perform accurate relative quantification. Efficient micelle removal was achieved through increased voltages applied in the HCD cell (150–200 V). No in-source activation was applied. The collision gas was Argon and pressure in the HCD cell was maintained at approximately 1×10^{-9} mbar.

Binding of POPG lipid and OBS1 to OmpF was performed as follows: Briefly, OBS1 peptide (NH$_2$-^{2}SGGDGRGHNTGAHSTSG^{18}-CONH$_2$) was diluted from a single stock to the desired concentration and mixed with equal volume of OmpF in 200 mM ammonium acetate with 1% (w/v) β-OG immediately before mass measurement. Conditions for nanoESI-MS were verified to generate spectra of sufficient quality to obtain resolved peaks without incurring ligand dissociation. 200 V was applied in the HCD cell with no additional in-source activation.

Data were processed using Thermo Scientific Xcalibur 2.1 and masses calculated using in-house software (http://benesch.chem.ox.ac.uk/resources.html). Proportions of the components in the mixtures were calculated by summing the intensities of the three lowest charge sates (18–20+) for each component. These were then divided by the sum of all the intensities for the three major peaks for all the series combined.

Current measurements and data analysis

Planar bilayers were formed from 1,2-diphytanoyl-sn-glycero-3-phosphocholine alone (DPhPC; Avanti Polar Lipids, Birmingham, AL) dissolved in pentane (Sigma Aldrich) or with a mixture with 1-palmitoyl-2-oleoyl-sn-glycero-3-phospho-(1'-rac-glycerol) (POPG; Avanti

Polar Lipids, Alabaster, AL, USA) dissolved in pentane/chloroform mixture (4:1, v/v) {Maglia, 2010 #1075}.

Both the cis and trans compartments of the apparatus contained 20 mM sodium acetate, 1 M KCl, pH 4.0 (1 mL), at 22.0 ± 1.5 °C. OmpF homotrimers (0.5 μL of 33.7 μM protein in 20 mM Tris-HCl (pH 8.0), 5 mM EDTA, 50 mM LiCl, 1 % (w/v) n-octyl-β-D-glucopyranoside) were added to the cis compartment (at ground) and incubated until a single porin had inserted into the bilayer. Currents were recorded by using a patch clamp amplifier (Axopatch 200B, Axon Instruments) at a holding potential of +100 mV with a sampling interval of 100 μs (10 kHz acquiring frequency) after the cis chamber had been perfused with 20 mM sodium acetate, 1 M KCl, pH 4.0, to remove excess protein. Events analysis was performed after low-pass filtering of the current traces at 100 Hz. Events shorter than 0.5 s or longer than 500 s were ignored.

Coarse-grained molecular dynamics simulations

The MemProtMD pipeline {Stansfeld, 2015 #1066} was used to set up MARTINI coarse-grained simulations {Monticelli, 2008 #1067} of AmtB (PDB:1U7G) and OmpF (PDB:2ZFG) in membranes composed of equal quantities of POPC and POPG. In order to simulate protonation of the lipids, the charge on the phosphate beads of POPC and POPG were changed from -1 to 0, resulting in a neutrally charged POPG and a positively charged POPC. Protonation of the protein was simulated by changing the charge of the sidechain beads of aspartic acid and glutamic acid from -1 to 0, and by changing the charge of a single sidechain bead of histidine from 0 to 1 . Deprotonation was simulated by giving histidine, arginine, and lysine sidechain beads a charge of 0. For each molecule, 20 independent coarse-grained self-assembly simulations were set up, five simulating a deprotonated system, five with only lipids protonated, five with only proteins protonated and five with the entire system protonated. Simulations were run for a total of 1 microsecond each and the first 200 nanoseconds discarded to allow the bilayer to self-assemble.

After a 200 ns equilibration, the final 800 ns of each simulation was performed using MDAnalysis (69). POPC or POPG head-groups within 0.6 nm of side-chains of acidic residues were identified as contacts, and numbers of contacts with POPC and POPG were calculated for each amino acid residue for each simulation frame. Preference for POPG was calculated as the number of frames for which a residue makes contact with a POPG head-group, divided by the number of frames in which a contact is made with head-groups of either lipid. A system-wide POPG preference was then calculated for each simulation as the mean of POPG preferences for all residues contacting lipids in at least 30% of frames. Means for each simulation in the deprotonated and protonated state (n = 5 per state) were compared using student's T-test.

Author Contributions

Competing financial interests

Acknowledgements

Corresponding authors

Correspondence to: Timothy M. Allison (timothy.allison@canterbury.ac.nz) or Carol V. Robinson (carol.robinson@chem.ox.ac.uk).
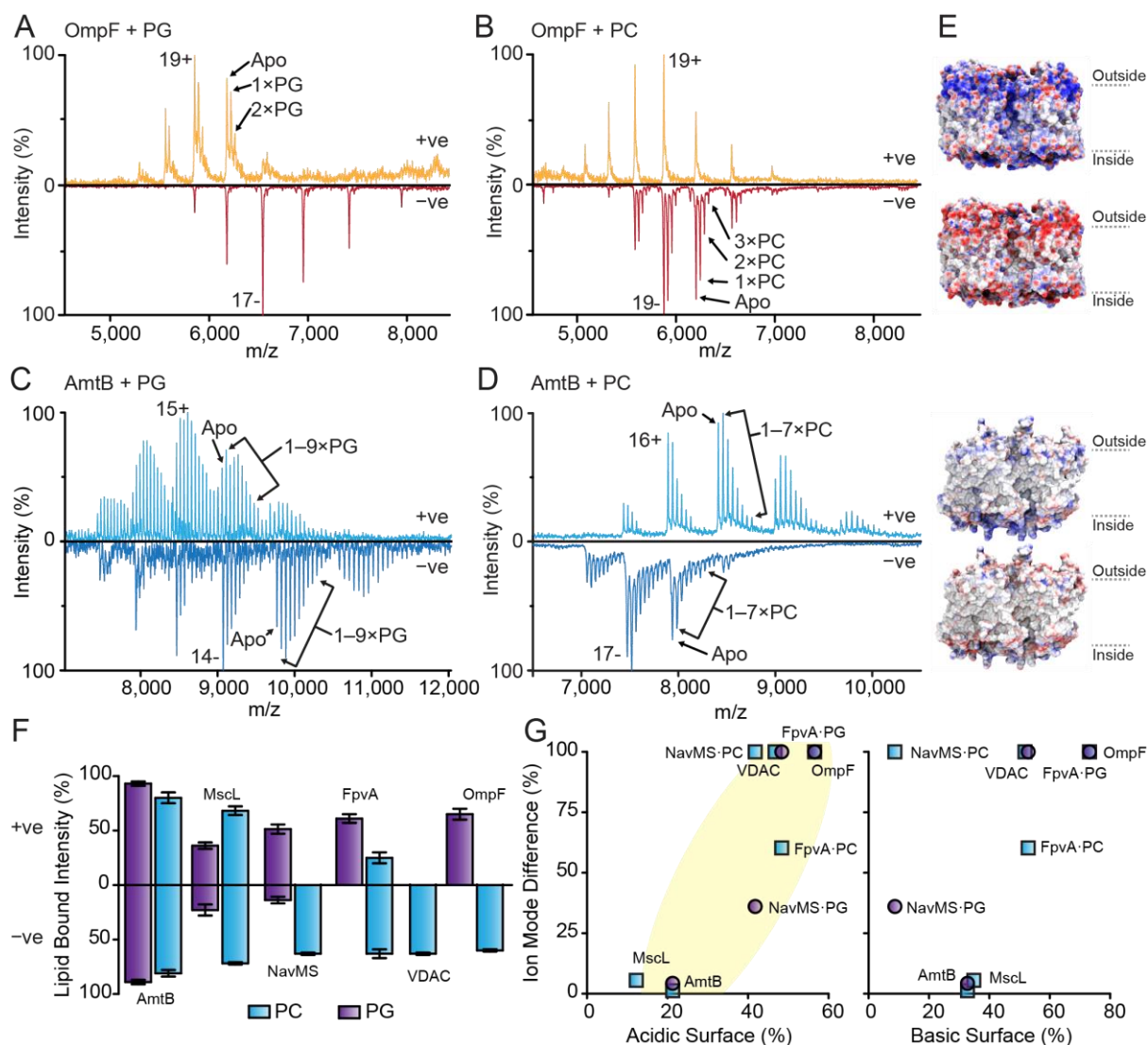
Figure 1: Native mass spectra of lipid binding to positively and negatively charged membrane proteins. (A)-(D) For each protein, spectra were recorded from the same electrospray needle under similar instrument activation conditions. The top spectrum in each panel was recorded in the positive electrospray polarity whilst the bottom spectrum was recorded with negative electrospray polarity. Discrete peaks are labelled, although in some cases more lipid binding is visible. (E) The corresponding protein surfaces coloured according to electrostatic charges at low and high pH for positive and negative ion modes respectively. The colour ranges were set from -20 (red) to 20 (blue). (F) Lipid binding as a percentage of the total intensity in positive (top) and negative (bottom) ion modes. Magnitude is dependent upon experimental conditions. (G) Relative difference in ion mode lipid binding percentage as a function of acidic (left) or basic (right) surface area. A positive correlation between acidic or basic residues and difference in lipid binding as a function of charge is observed for acidic residues (highlighted yellow).
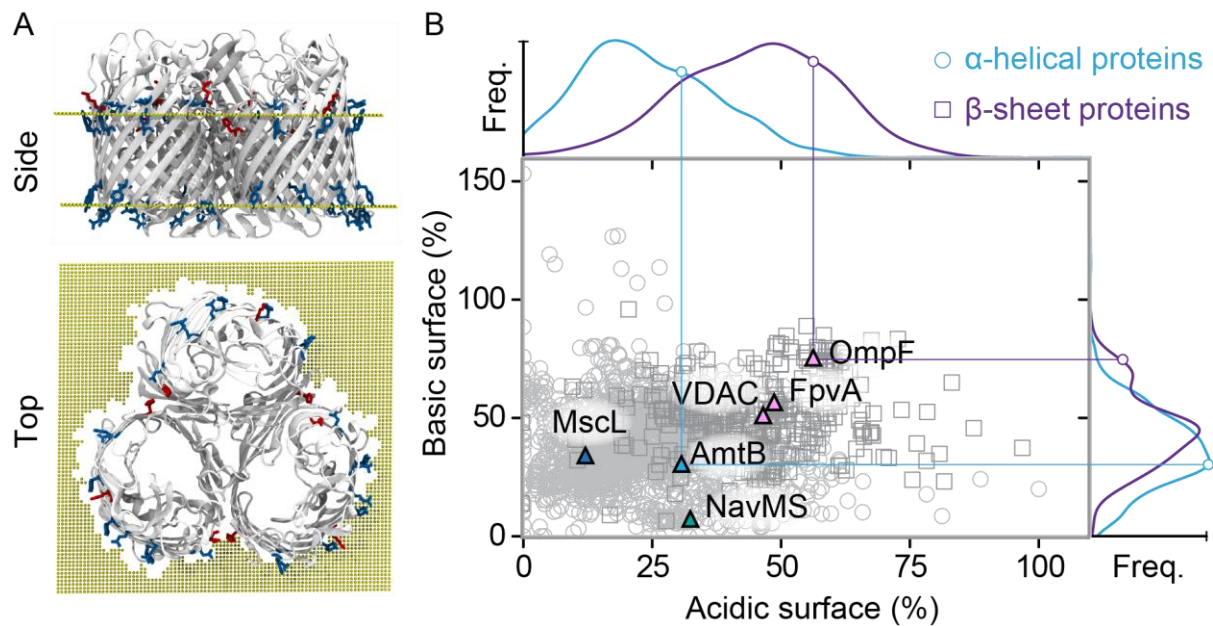
Figure 2: Analysis of structures in the Protein Data Bank of Transmembrane (PDBTM) to determine the surface area contribution of acidic and basic residues to the lipid head group binding region. (A) The analysis process first aligned each membrane protein structure to determine the region of the protein proximal to the lipid head groups in a lipid bilayer. The proportion of the surface area of this region contributed by either acidic or basic residues was calculated. (B) All membrane protein structures analysed (n=2064) for acidic and basic residue contribution. β-sheet/outer membrane proteins (grey squares) have more acidic or basic residues in the lipid head group binding region than α-helical membrane proteins (grey circles). The surface area contribution was calculated for both the inside and outside lipid head group binding regions and these two values were summed for each protein. The set of annotated outer membrane proteins is identical to those classified as β-sheet, with the exception of the addition of structures of hemolysin. Membrane proteins analysed by native MS to investigate lipid binding are independently plotted (triangles) and coloured according to the protein type (α-helical green, β-sheet pink). The locations of AmtB and OmpF are denoted. Axes are decorated with histograms (bin size of 2) of distribution of proteins with different surface area contributions, smoothed by applying a kernel-density estimate using Gaussian kernels.
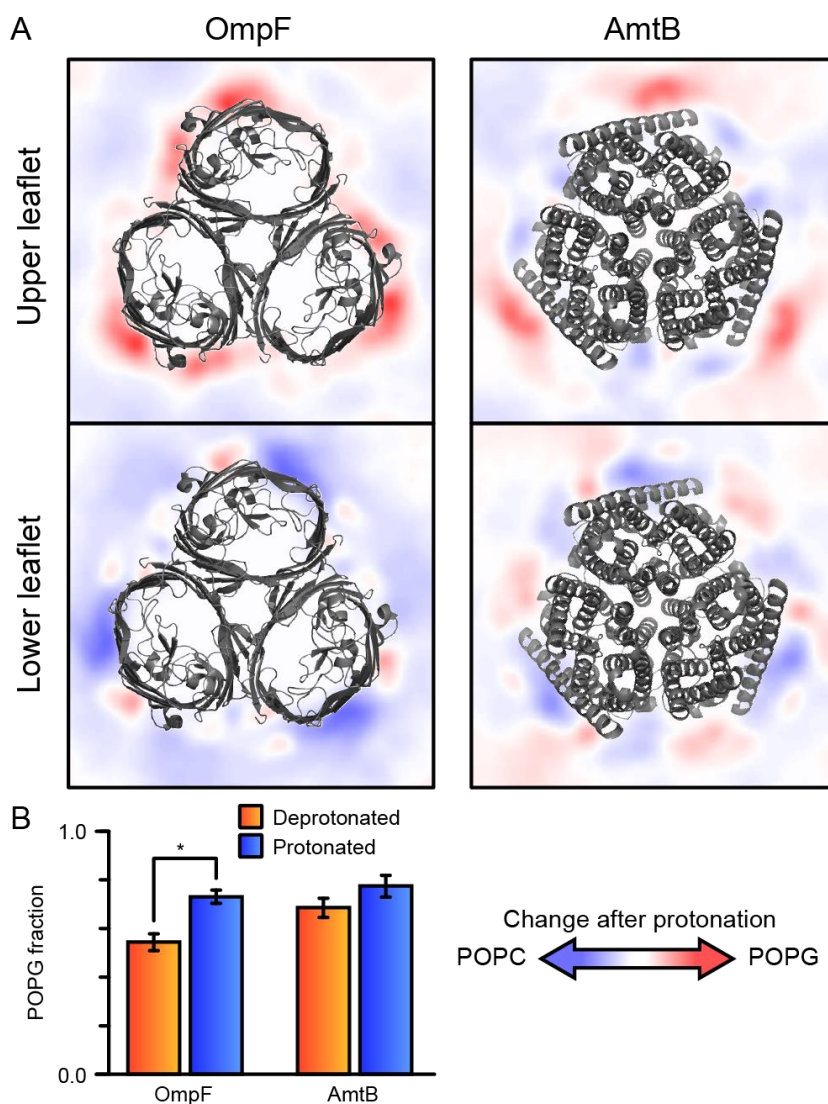
Figure 3: Coarse-grained molecular dynamics simulations of AmtB and OmpF in mixed bilayers of POPC and POPG. (A) Changes in lipid binding preferences after protonation. The membrane proteins are in a cartoon representation coloured grey. (B) The relative binding preferences for POPG (over POPC) calculated as the fraction of total lipid occupancy for OmpF and AmtB towards acidic residues in different protonation conditions. Errors bars represent standard deviation from five simulations. The change in POPG fraction for OmpF is significantly different (p-value < 0.0001) as indicated by *, whereas in the case of AmtB the change in POPG fraction prior and after protonation was not statistically different (p-value < 0.74).
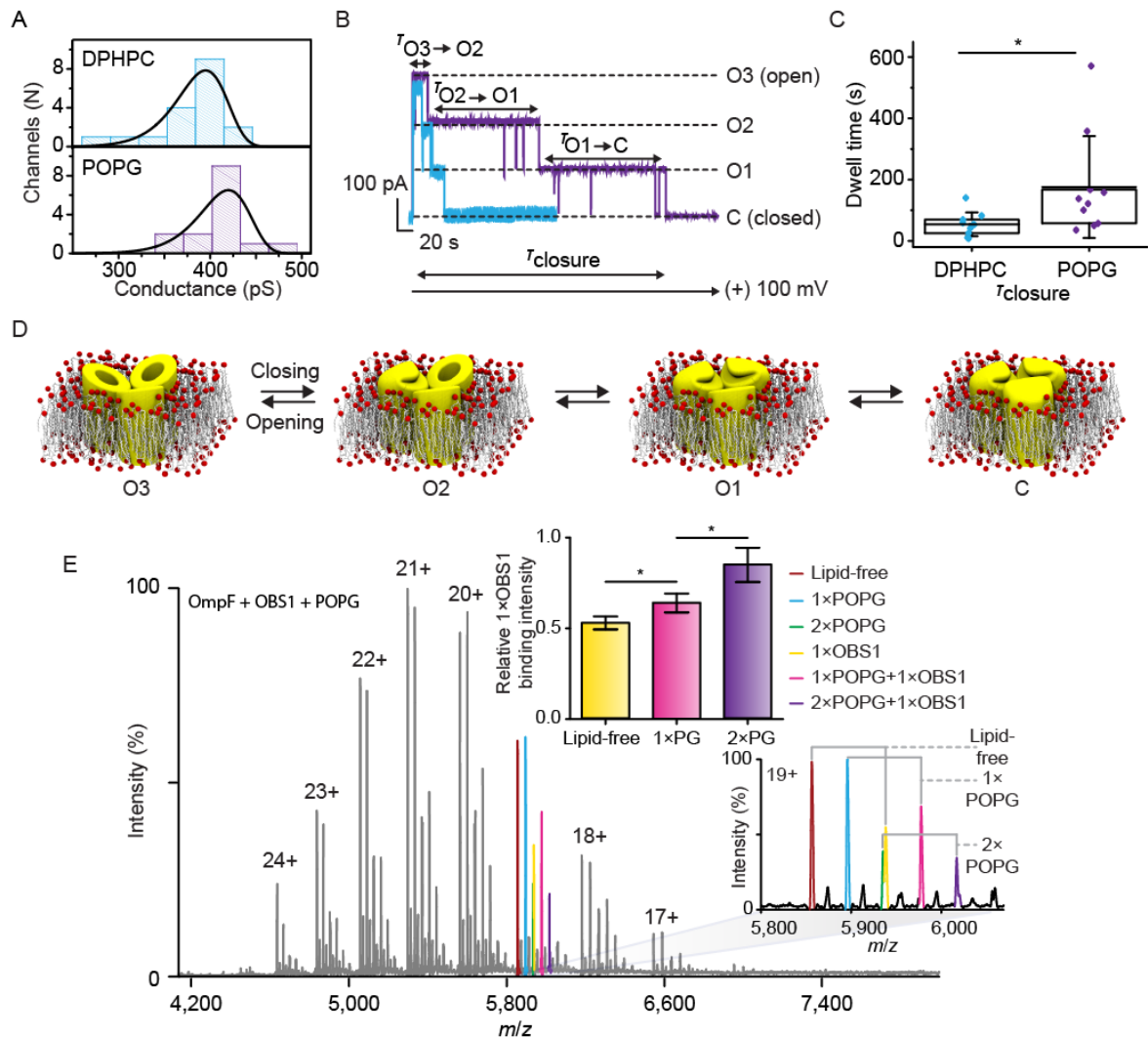
Figure 4: The influence of the negatively charged lipid, POPG, on OmpF porin gating at low pH. (A) OmpF channel conductance values (all three pores open) in 1 M KCl at pH 4.0 at +100 mV were obtained in DPhPC planar bilayers (blue) and in DPhPC/POPG (3:1 ratio) bilayers (purple) with 19 and 15 independent OmpF porins, respectively. The mean conductance value of the fully open OmpF channel was 1.3 ± 0.2 nS (n = 19) per monomer in a DPhPC bilayer and 1.4 ± 0.1 nS (n = 15) in a DPhPC/POPG bilayer. (B) Representative current versus time traces for a single OmpF porin in a DPhPC bilayer (purple) and in a DPhPC/POPG (3: 1) bilayer (blue). A trans potential of +100 mV was applied until all the pores had closed. (C) Box and whisker plot of closure times. The top and bottom lines of a box enclose values in the range encompassing 25% to 75% of the values. The mean closure times are shown as black lines within the boxes and are significantly different as determined by Mann Whitney test (p-value < 0.021). (D) Schematic showing stepwise OmpF gating. The resulting states of OmpF are O3 (three pores open), O2 (two pores open), O1 (one pore open), and C (all closed). (E) High-resolution native MS of OmpF in the presence of OBS1 (10 µM) and POPG (100 µM) (left). A range of bound forms are observed in the spectrum of single and double peptide and lipid binding combinations. Inset: expansion of charge state 19+. Bar chart of relative peak intensities indicates that peptide co-bound with POPG is observed to a greater extent than bound alone. The mean relative binding intensities are significantly different in the different lipid bound forms (*p*-values of 0.0008 and 0.027)

References

Lipid binding attenuates channel closure of the outer membrane protein OmpF

Idlir Liko[1,2], Matteo T. Degiacomi[1†‡], Sejeong Lee[1‡], Thomas D. Newport[2], Joseph Gault[1], Eamonn Reading[1⊥], Jonathan T.S. Hopper[1,2], Nicholas G. Housden[3], Paul White[3], Matthew Colledge[4], Altin Sula[4], Bonnie A. Wallace[4], Colin Kleanthous[3], Phillip J. Stansfeld[3], Hagan Bayley[1], Justin L.P. Benesch[1], Timothy M. Allison[1*•] and Carol V. Robinson[1,2*]

1 Department of Chemistry, University of Oxford, South Parks Road, Oxford, OX1 5QY, UK

2 OMass Technologies, Begbroke Science Park, Kidlington, OX5 1PF, UK

3 Department of Biochemistry, University of Oxford, South Parks Road, Oxford, OX1 3QU, UK

4 Institute of Structural and Molecular Biology, Birkbeck College, University of London, Malet Street, London, WC1E 7HX, UK

⊥ Current address: Department of Chemistry, Kings College London, Britannia House, 7 Trinity Street, London, WC2R 2LS, UK

† Current address: Chemistry Department, Durham University, South Road, Durham, DH1 3LE, UK

• Current address: Biomolecular Interaction Centre and School of Physical and Chemical Sciences, University of Canterbury, Christchurch, NZ

‡ These authors contributed equally to this work

Supplementary methods

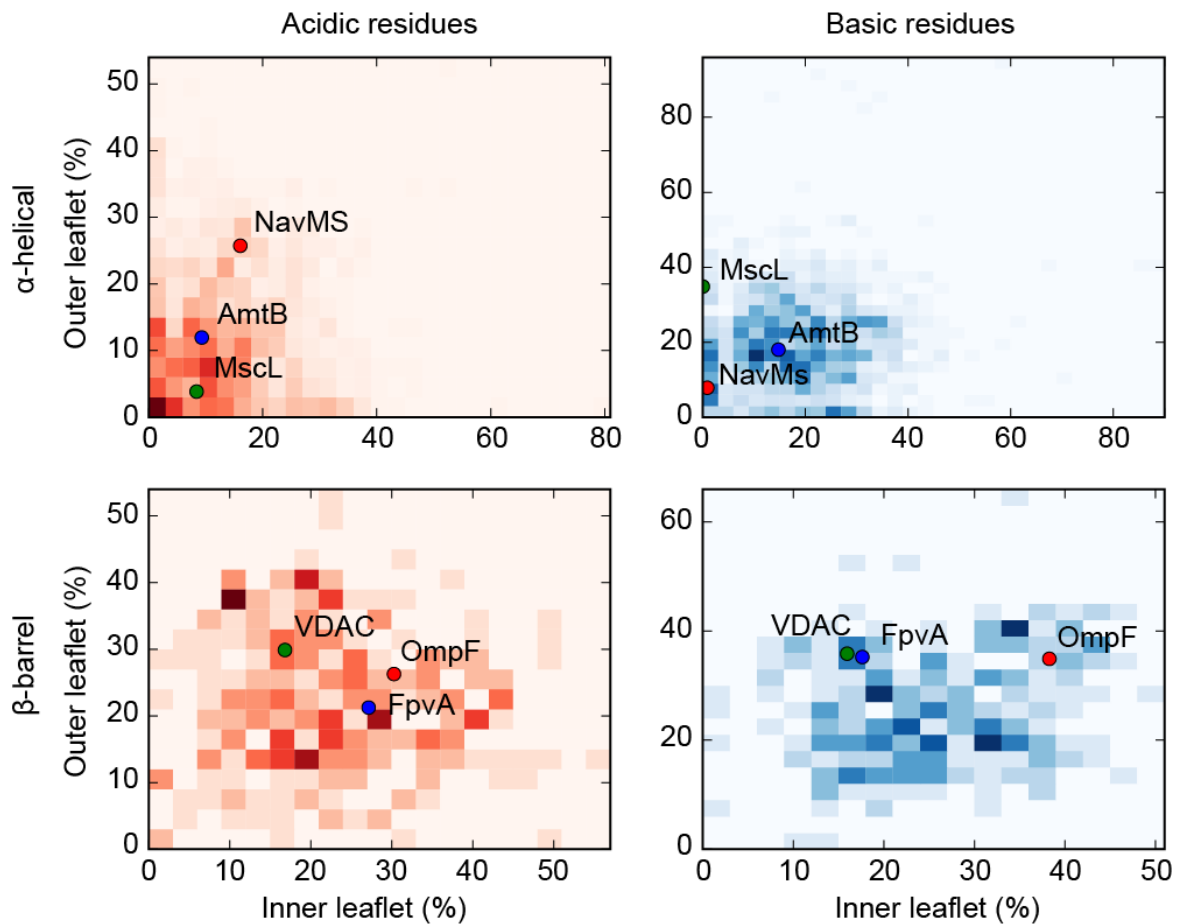**Analysis of lipid head group binding regions of membrane protein structures**

The following steps were taken to effect this analysis:

1) Build a dense point mesh (1 Å spacing) around the protein's head group region, representing lipid head groups' location. On x and y axis, the mesh is large enough to encompass all the protein atoms. For inner leaflet, $z=[-z_{PDBTM}-t, -z_{PDBTM}]$, for outer leaflet $z=[z_{PDBTM}, z_{PDBTM}+t]$, where $t=3$ Å mesh thickness along z axis.
2) Remove from the mesh all points at less than $c=1$ Å from the protein, where c is a clashing distance threshold.
3) Launch a DBSCAN {Ester, 1996 #1069;Pedregosa, 2011 #1070} clustering algorithm on the remaining points. This algorithm considers contiguous points as part of the same cluster. Select only the points sharing the cluster with a mesh corner point: as a result, the selected points completely encircle the protein, without clashing with it. Thus, if the protein is a channel, points located in its central cavity are now removed.
4) Detect all protein atoms within $d=4$ Å from the mesh, and compute their solvent accessible area ($SASA_{all}$) using Shrake-Rupley ("rolling ball") algorithm. Between these atoms, identify the subset part of basic or acidic amino acids. Compute the SASA of both these subsets, and the resulting presence ratios $\rho_{acidic}=SASA_{acidic}/SASA_{all}$ and $\rho_{basic}=SASA_{basic}/SASA_{all}$.

As a result of following this protocol, every protein is characterized by four numbers, i.e. the presence ratio of basic and acidic amino acids on bottom and top leaflet of the bilayer. This protocol is controlled by three parameters, mesh thickness t, mesh clash distance c and protein-mesh contact distance d. To assess the sensitivity of our protocol to these parameters several runs with different parameter sets were performed, namely $[t,c,d]$ = [3, 3, 5], [5, 3, 5], [3, 2.5 ,5], [3, 3.5, 5], [6, 3.5, 5], [6, 3, 5]. By computing mean and standard deviation of all resulting ρ scores, 6.8% of performed measures had a standard deviation above 5 (0.5% above 10). These cases were inspected manually: the difference was always caused by a misdetection of internal cavity by one of the different methods. Parameters used in this work have been chosen as those displaying the smallest deviation from mean.
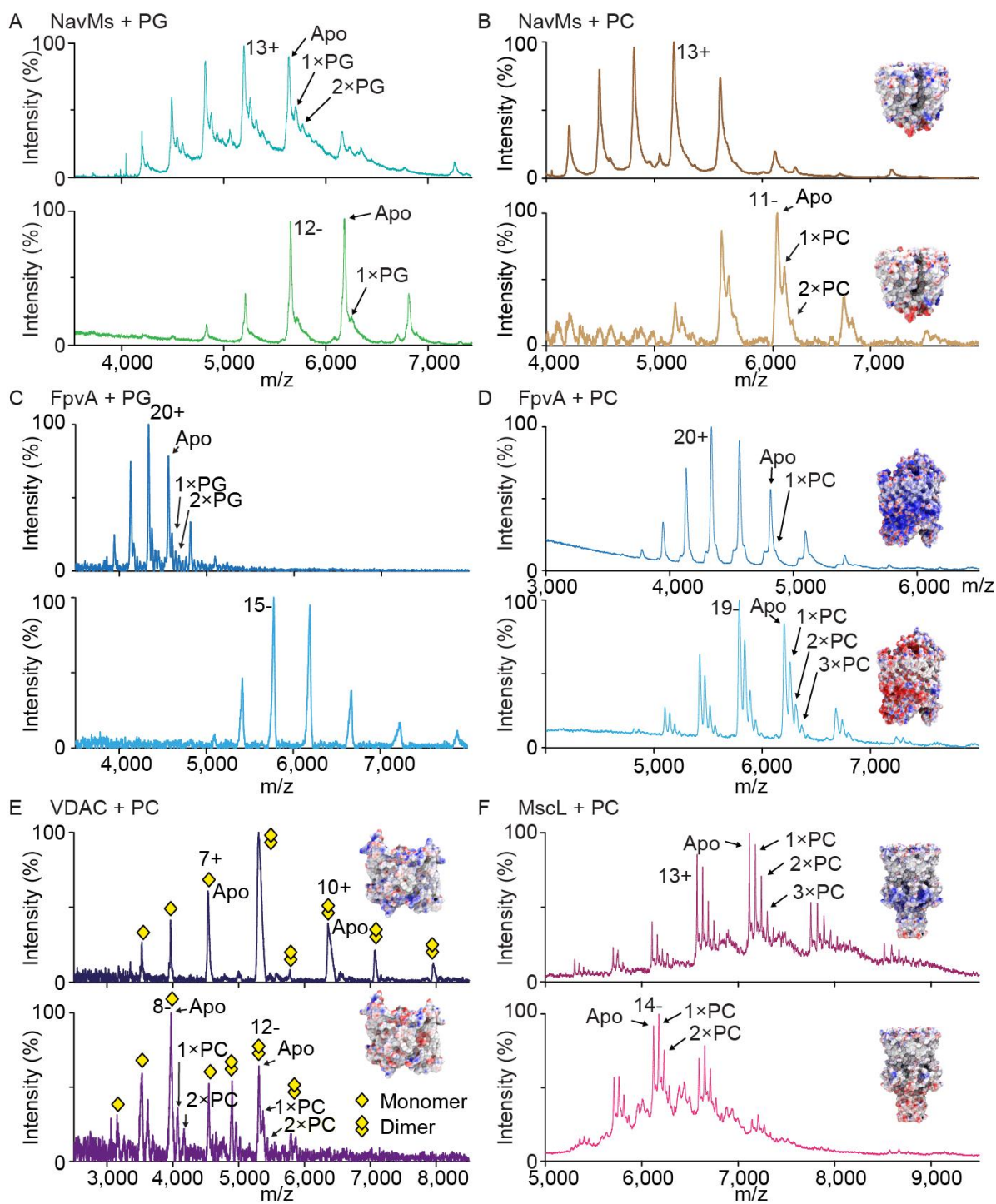
Figure S1: Mass spectra of membrane proteins in the presence of POPG and POPC in different ion modes (positive top, negative bottom in each panel). Both monomeric and dimeric forms of VDAC are observed in the mass spectra, with similar lipid binding behaviour (C). Inset: electrostatic surface of VDAC at low and high pH for positive and negative ion modes respectively. The colour range is set from -20 (red) to 20 (blue).

Figure S2: Analysis of acidic and basic residues in the lipid head group binding regions of membrane protein structures. The surface area contributions for the inside and outside leaflets is plotted as a 2D-histogram (bin size of 3), of either acidic or basic residues for α-helical and β-sheet membrane proteins. Generally, the surface area contribution is not correlated to either a symmetric, or an asymmetric distribution between the two sides of the membrane proteins. The values for membrane proteins studied here are plotted independently.
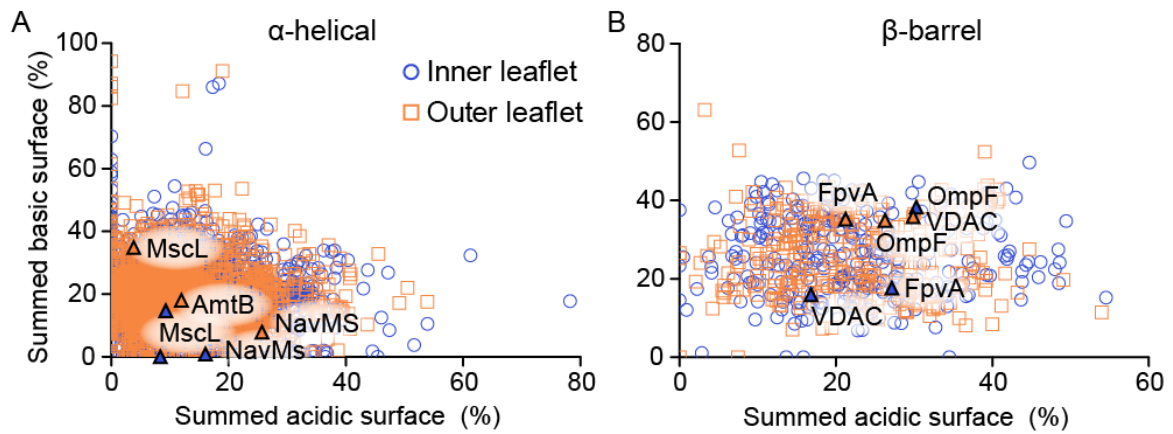
Figure S3: Analysis of surface area contribution to the lipid head group binding region by acidic or basic residues for different protein types and inner and outer leaflets. The distribution of acidic or basic residues, for both membrane protein types, is similar for the regions of the proteins corresponding to the inner and outer membrane leaflets. The values for membrane proteins studied here are plotted independently as triangles.
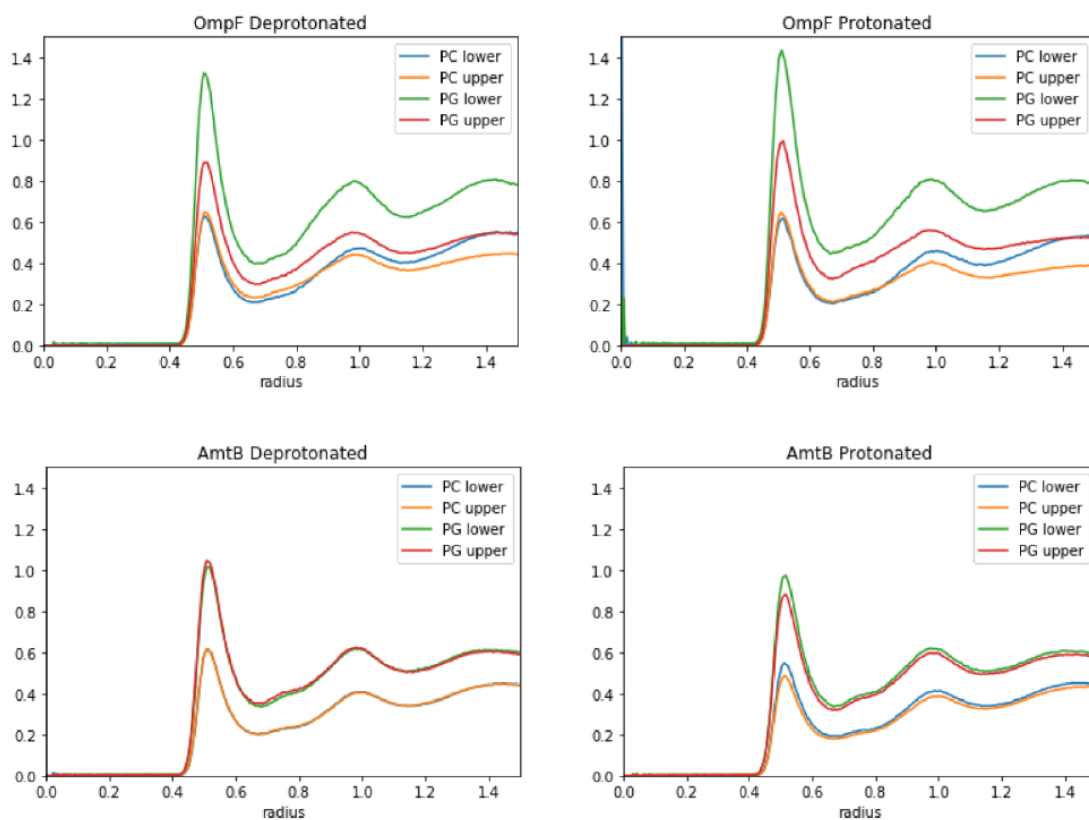
Figure S4: Lipid density of POPC and POPG in upper and lower leaflets as a function of radius (Å) from AmtB and OmpF under different protonation conditions. For OmpF a higher density of PG is observed in both the upper and lower leaflets while for AmtB differences between PC and PG are less marked.
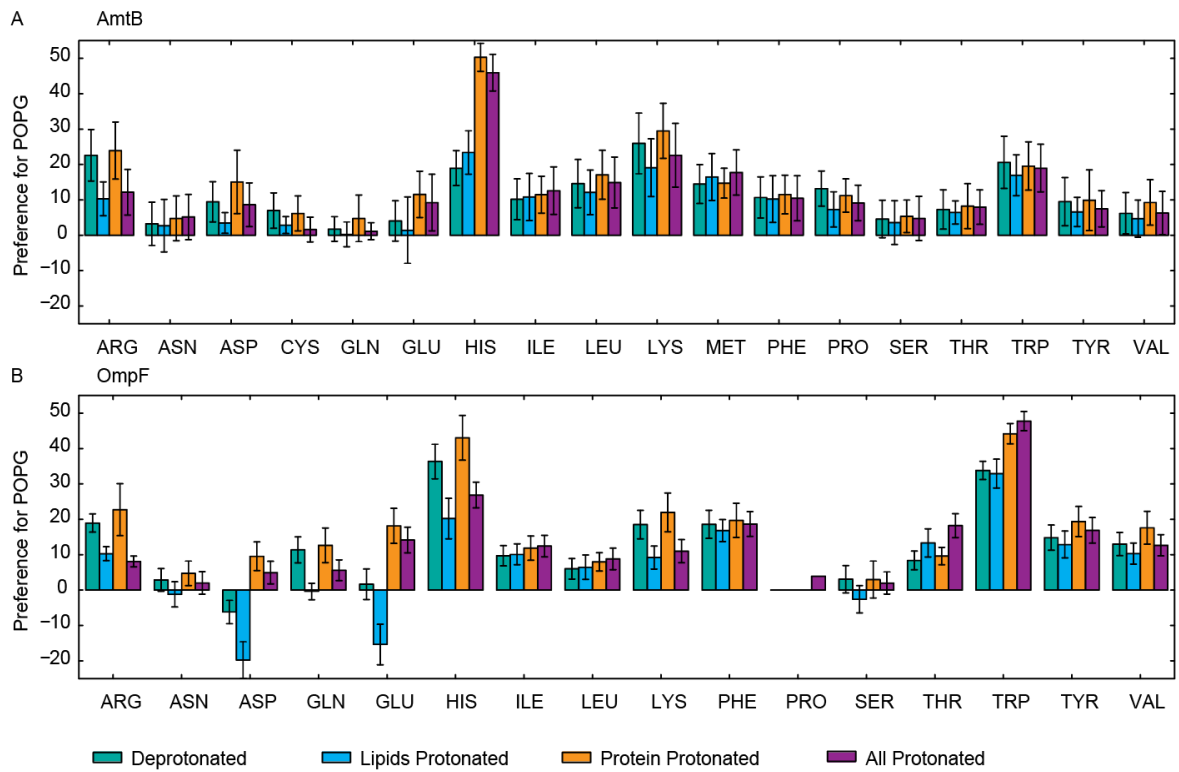
Figure S5: Coarse-grained molecular dynamics simulations of AmtB and OmpF.
Relative preference for POPG per residue for each protein under different protonation
conditions.
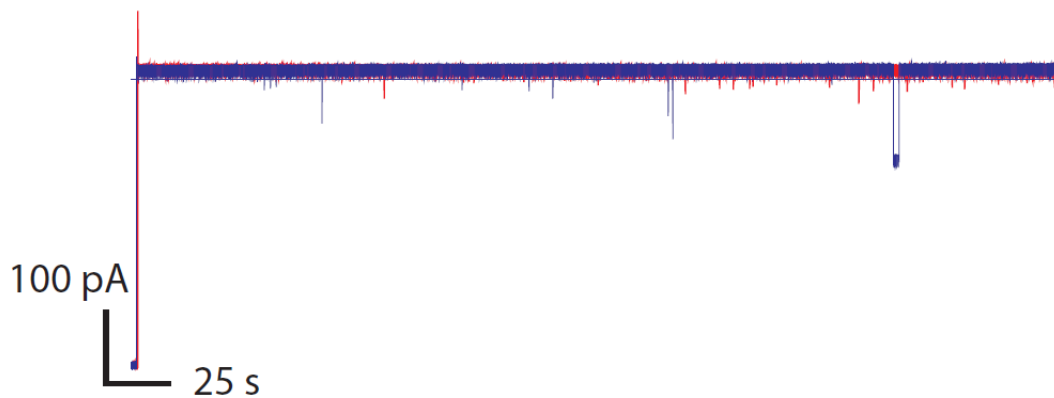
Figure S6: Influence of the negatively charged lipid, POPG, on OmpF channel gating at pH 8.0. Representative current versus time traces for a single OmpF porin in a DPhPC bilayer (red) and in a DPhPC/POPG (3:1) bilayer (blue). The porin was observed at +100 mV for approximately six minutes, as previously carried out at pH 4.0. Both in the presence and the absence of POPG, the OmpF porin shows only a fully open state (n = 5, respectively).

Similar conductance values were obtained in DPhPC planar bilayers and in DPhPC/POPG (3:1 ratio) bilayers (n = 5). The mean conductance values are: DPhPC, 4.2 ± 0.4 nS; DPhPC/POPG, 4.1 ± 0.4 nS, in 20 mM potassium phosphate, 1 M KCl buffer. Because the gating of OmpF at pH 8.0 was rarely observed over the period of measurement, dwell times could not be measured and analysed. Over the same period at pH 4.0, sufficient data could be recorded.
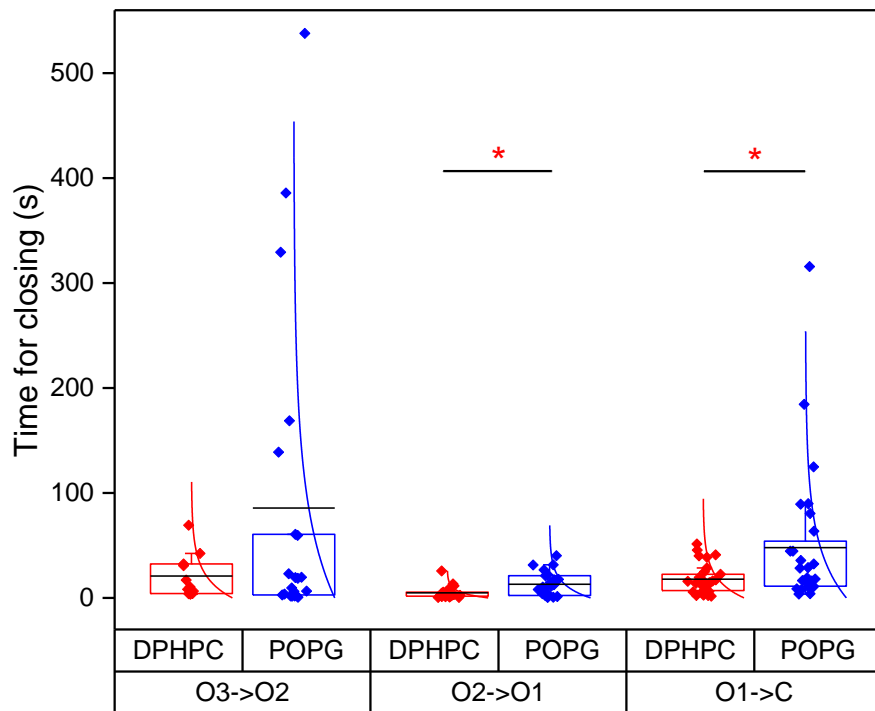
O3 -> O2		O2 -> O1		O1 -> C	
DPhPC	DPhPC/POPG	DPhPC	DPhPC/POPG	DPhPC	DPhPC/POPG
20.9 ± 20.0 (n=11)	85.5 ± 146.3 (n=18)	4.90 ± 5.6 (n=22)	13.1 ± 11.1 (n=23)	17.9 ± 13.6 (n=29)	48.0 ± 66.0 (n=29)

Figure S7: Influence of the negatively charged lipid, POPG, on OmpF channel gating (closing) at pH 4.0.

The voltage-induced gating of OmpF was observed at +100 mV in the absence and the presence of POPG lipids. Closure times in each step are shown as box-plots in logarithmic scale. The top and bottom lines of a box enclose values in the range encompassing 25% to 75% of the values. The mean closure times are shown as black lines. Statistically significant differences are seen in two closing step ($\tau_{O2->O1}$, $\tau_{O1->C}$), whose *p*-values are 0.015 and 0.044, respectively, and marked with an asterisk. Data were fitted with an exponential function to define the probability density function (pdf) and ß-value, which is the mean, as shown in the table.

.
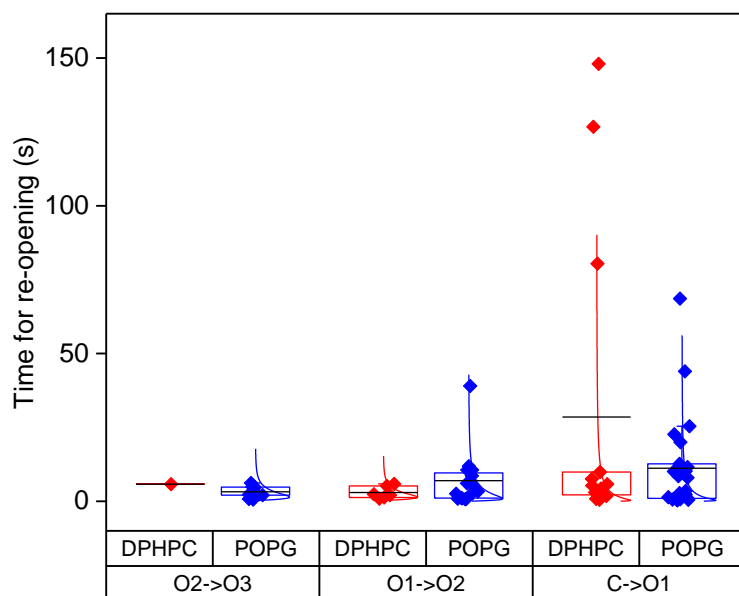
| O2 -> O3		O1 -> O2		C -> O1	
DPhPC	DPhPC/POPG	DPhPC	DPhPC/POPG	DPhPC	DPhPC/POPG
5.8 (n=1)	3.2 ± 1.8 (n=10)	3.0 ± 1.9 (n=6)	7.0 ± 8.9 (n=16)	28.5 ± 50.1 (n=14)	11.2 ± 16 (n=23)

[ ]

Figure S8: Influence of the negatively charged lipid, POPG, on OmpF channel gating (re-opening) at pH 4.0.

Re-opening of OmpF was observed at +100 mV in the absence and the presence of POPG lipids. Re-opening times in each step are shown as box-plots in logarithmic scale. The top and bottom lines of a box enclose values in the range encompassing 25% to 75% of the values. The mean closure times are shown as black lines. Data were fitted with an exponential function to define the probability density function (pdf) and ß-value, which is the mean, as shown in the table.
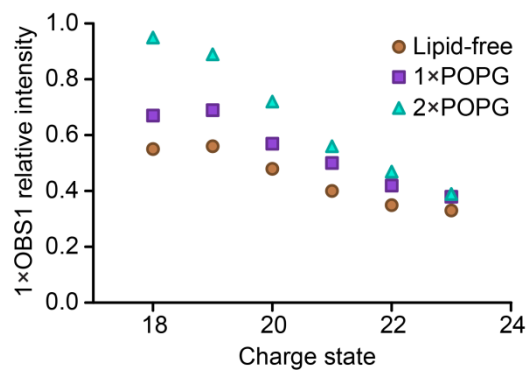
Figure S9: Relative peak intensities of OBS1-bound forms across charge states. Peak intensities are from the spectrum in Fig. 4 and are the maxima of each peak in the normalised raw data. The lowest charge states, 18+ and 19+, show the least charge-state dependence on relative intensities. Notably the relative increase in intensity of OBS1 binding to POPG forms compared to lipid-free forms shows little charge-state variation, whilst binding to 2×POPG forms shows charge-state variation across all states.
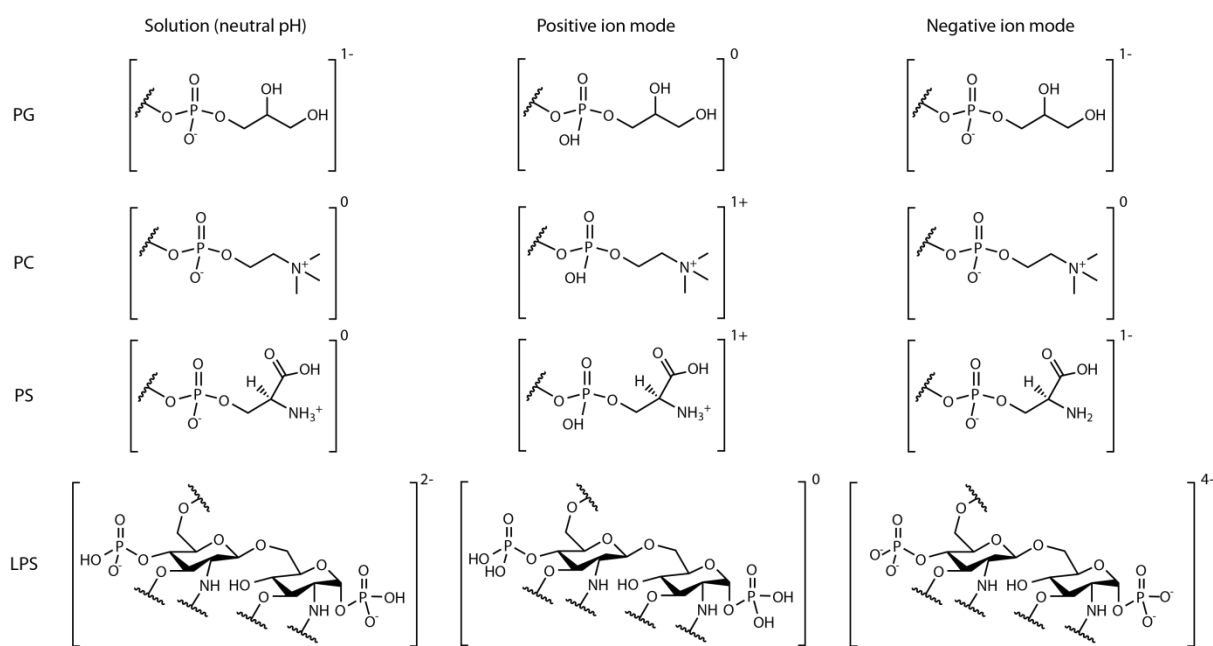
Figure S10: The chemically distinct headgroups of PG, PC, PS and LPS. The expected net charge on the lipids in solution and different mass spectrometry ion modes are annotated.

Table S1: Surface areas of acidic and basic residues for selected proteins.

Protein	PDB files	Average Acidic (%)			Average Basic (%)		
		Inside	Outside	Total	Inside	Outside	Total
AmtB	2NS1, 1U7G, 2NUU, 1U77, 3C1G, 3C1H, 3C1J, 2NMR, 2NOP, 2NOW, 2NPC, 2NPD, 2NPE, 2NPG, 2NPJ, 2NPK, 1XQE, 1XQF, 1U7C, 4NH2	9.3	12.0	21.3	14.7	18.0	32.7
MscL	2OAR	8.4	3.9	12.3	0	34.9	34.9
FpvA	2W16, 2W6T, 2W6U, 2W75, 2W76, 2W77, 2W78, 2O5P, 2IAH, 1XKH	27.1	21.2	48.3	17.6	35.2	52.8
OmpF	4GCP, 4GCQ, 4GCS, 4LSE, 4LSF, 4LSH, 4LSI, 4JFB, 3POQ	30.3	26.3	56.6	38.3	34.9	73.2
NavMs	4OXS, 4P2Z, 4P9O, 4P9P, 4PA3, 4PA4, 4PA6, 4PA7, 4PA9, 4CBC, 3ZJZ	16.1	25.7	41.8	0.9	7.9	8.8
VDAC	2JK4	16.8	29.9	46.7	15.9	35.9	51.8

Table S2: Rate constants for opening and closing steps. Rate constants were calculated directly by taking the inverse of the mean dwell time, for the first subunit lcosing (k_1) and the first subunit re-opening (k_6).

Closing rates	k_1 ($10^{-2}s^{-1}$)(O3 -> O2)	Re-opening rates	k_6 ($10^{-1}s^{-1}$)(C -> O1)
DPhPC	4.8 ± 4.6	DPhPC	0.4 ± 0.6
DPhPC/POPG	1.2 ± 2.0	DPhPC/POPG	0.9 ± 1.3